CHAPTER – 4
EXPERIMENTAL METHOD

4.1 Materials

This chapter deals with the materials used, methods of preparation of CSNPs, instrumental techniques used for the structural, dielectric and magnetic studies of the prepared CSNPs and other experimental procedures for carrying out the research work. The researcher has synthesised five types of heterogeneous core-shell nanocomposites using liquid phase synthesis technique, the materials are,

(i) Fe_2O_3-Gd_2O_3 CSNPs

(ii) $NiFe_2O_4$-Gd_2O_3 CSNPs

(iii) Gd_2O_3-$NiFe_2O_4$ CSNPs

(iv) Gd_2O_3-NiO CSNPs

(v) Fe_2O_3-$Ca_{10}(PO_4)_6.(OH)_2$ CSNPs

The chemicals used for the synthesis of all the above five type of CSNPs are the purest research grade. Double distilled water and ethanol were employed for the washing procedure. The chemicals used for the synthesis in the present work are listed in Table 4.1.

Table 4.1 Chemicals used in the present work

S. No	Name of the chemical	Chemical formula	Company name	Country
1.	Iron (II) sulfate heptahydrate (GR)	$FeSO_4.7H_2O$	Merck	India
2.	Iron (III) chloride anhydrous purified	$FeCl_3$	Merck	India
3.	Nickel (II) nitrate hexahydrate	$Ni(NO_3)_2.6H_2O$	Alfa Aesar	USA
4.	Gadolinium nitrate hexahydrate	$Gd(NO_3)_3.6H_2O$	Alfa Aesar	USA
5.	Calcium nitrate tetrahydrate purified LR	$Ca(NO_3)_2.4H_2O$	S. D. Fine Chemicals	India
6.	Ortho phosphoric acid GR	H_3PO_4	Central Drug House	India
7.	N-Cetyl N, N, N-tri methyl ammonium bromide (CTAB)	$C_{19}H_{42}BrN$	Otto Chemicals	Japan
8.	Polyethylene glycol 400 (PEG)	$C_{2n}H_{4n+2}O_{n+1}$, n=8.2 to 9.1	SRL Chemicals	India

4.2 Methods

4.2.1 Polyol Process

Several methods have been developed to synthesis of core-shell nanosystems. Among them, polyol is an efficient and easy method to synthesis of metal oxide based CSNPs. In this method, polyalcohols act as a reaction medium and also a reducing agent. Materials prepared from this method possess high crystalline nature due to the reaction temperature is higher than the room temperature.

The polyol process refers to a polyalcohol that acts not only as a solvent but also as a mild reducing agent, it serves as a perfect medium for the reduction of metal salt precursors. In this process, a solid inorganic precursor is suspended in a liquid polyol. The suspension is stirred and heated to a given temperature, which can reach the boiling point of the polyol for less easily reducible oxide particles. The alcohol itself acts as a stabilizer, limiting particle growth and prohibiting agglomeration. Due to the high temperatures which can be applied (>150 ^{o}C), often highly crystalline oxides are yielded. Moreover, the synthesis is comparably easy to perform. A better control of the average size of the metal particles can be obtained by seeding the reactive medium with foreign particles (heterogeneous nucleation). In this way, nucleation and growth steps can be completely separated and uniform particles are obtained. Beside oxides, a variety of materials including sulfides, phosphates, as well as elemental metals were yielded based under very similar experimental conditions [1-4]. The starting materials can range from hydroxides (eg: $Cu(OH)_2$), nitrates (eg: $AgNO_3$), oxides (eg: Cu_2O), chlorides (eg: $FeCl_3$) to acetates (eg: $Ni(CH_3COO)_2$). The reduction to metal oxide can be achieved in various polyols such as ethylene glycol, propylene glycol, diethylene glycol, trimethylene glycol, butylene glycol and trimethylene glycol (Figure 4.1).

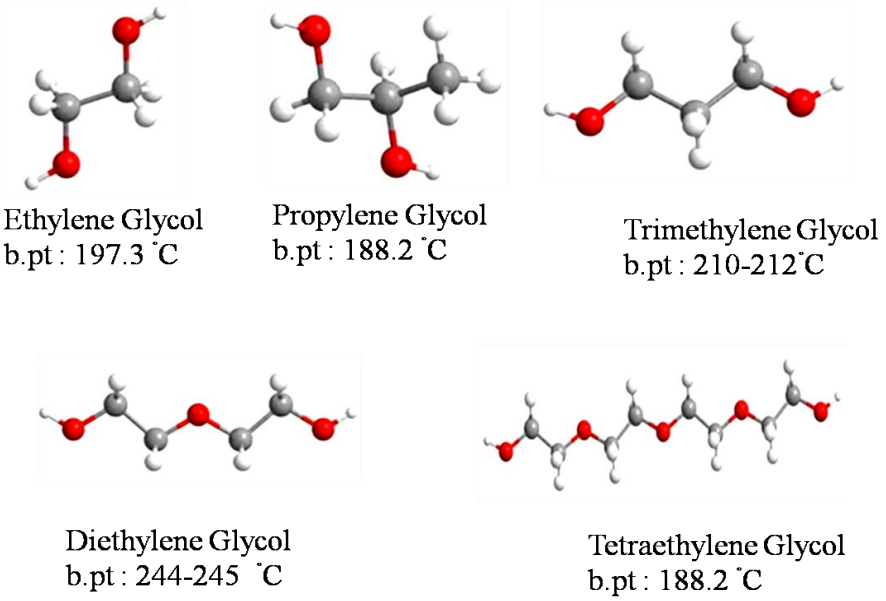

Figure 4.1 Various polyols used for the reduction of metal salt precursors along with their corresponding boiling point (b.pt)

Different polyols are chosen depending on the reduction potential of the metal oxides. The easily reducible metal oxides do not require high heat, that can be reduced in butylene glycol, while less easily reducible metal oxides require higher temperatures and tetraethylene glycol is required. Fievet *et al*. [5] proposed that the reduction of metals in a liquid polyol medium occurs by dissolution of the metal salt precursor, reduction by the polyol of the dissolved species and nucleation and growth of the metal particles from the solution. Joseyphus *et al*. [6] evaluated several factors governing the production yield of Fe particles like type of polyols, ferrous salts, ferrous ion concentration, hydroxyl ion concentration and reaction temperature. He found out the yield and size of Fe particles varied depending upon the reduction potential of the polyols. The solvents as polyols for example, polyethylene glycol, offer interesting properties, owing to their high dielectric constants, they act as solvents able to dissolve inorganic compounds and owing to their relatively high boiling points, they offer a wide operating-temperature range (from 25 °C to the boiling point) for preparing inorganic compounds. Figure 4.2 represents the flow chart for the synthesis of nanomaterials by polyol method.

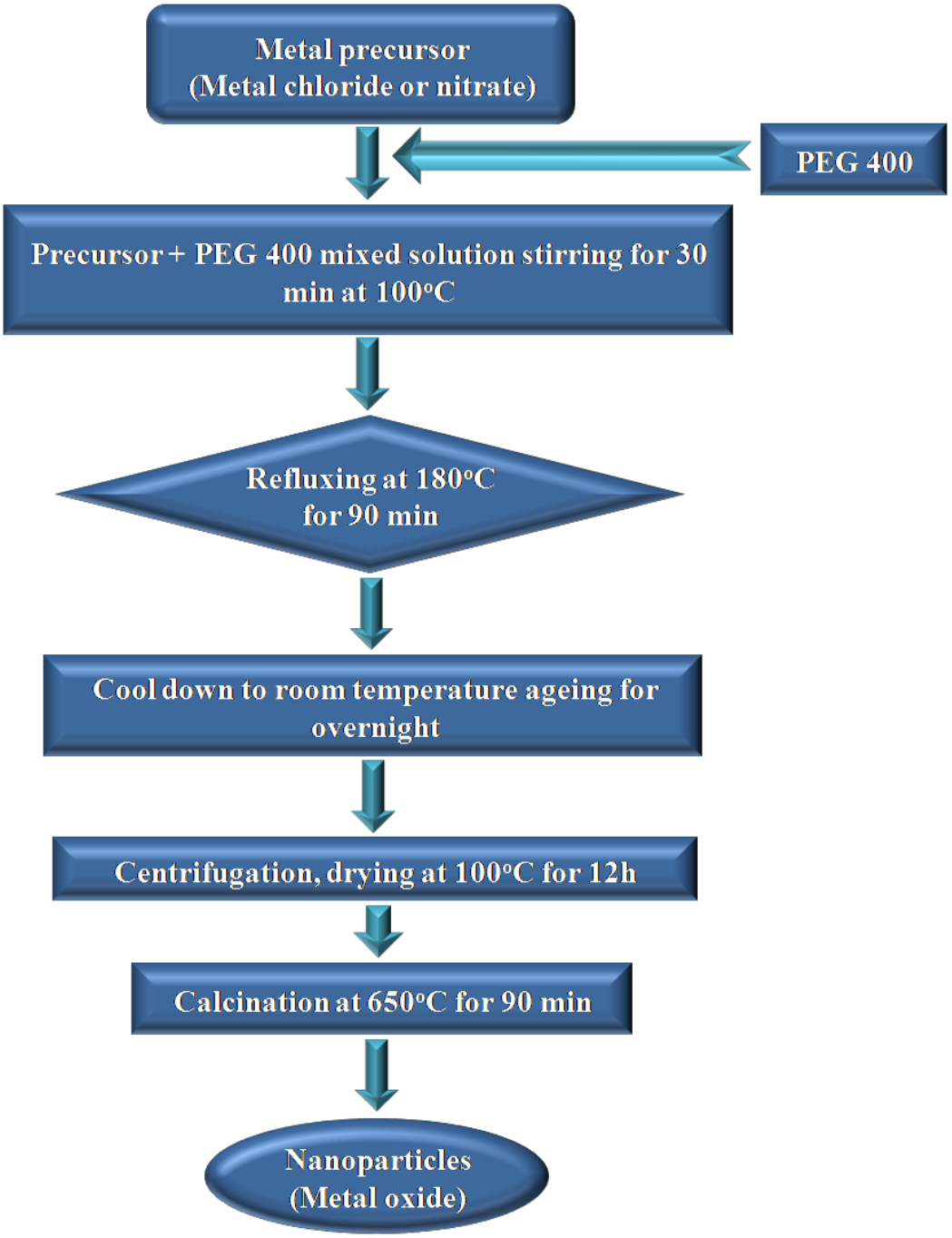

Figure 4.2 Flow chart of the polyol synthesis process

4.2.2 Co-precipitation method

Co-precipitation from aqueous or organic solutions has been used in most of the methods. A size range of 30 to 100 nm particles can be obtained by the reaction of a metal salts, a base and a mild oxidant (nitrate ions) in aqueous solutions [7]. The phase and size of the particles depend on the concentration of cations, the counter ions present and the pH of the solution [8]. By altering the pH and the ionic strength, mean size of the particles can be controlled (from 15 to 2 nm) [9-11]. Nanoparticles are likely to aggregate because of large surface area to volume ratio to reduce their surface energy [12]. The suspension of NPs can be stabilized by adding anionic surfactants as dispersing agents [13, 14]. Stabilization can also be achieved by coating the particle surfaces with proteins [15-17], starches [18, 19], non-ionic detergents [13] or poly electrolytes [12]. Adsorption of such substances stabilizes the particles at electrolyte concentrations, otherwise it would be high enough for coagulation to occur [20, 21]. Co-precipitation reaction involves the simultaneous occurrence of nucleation, growth, coarsening, and/or agglomeration. A detailed description of particle growth is given below.

4.2.2.1 Nucleation

The precipitation involves nucleation, where the driving force is the change in chemical potential between standing and equilibrium states. The most common method to generate supersaturation is by reactive precipitation, when a chemical reaction produces insoluble species. The supersaturation in precipitation is often very high and giving rise to high nucleation rates. The chemical reactions used to induce co-precipitation can take numerous forms. Consider the case of a simple addition reaction for the formation of an electrolyte, A*x*B*y*:

$$_{X}A^{Y+}\,(aq) + {}_{Y}B^{X-}\,(aq) \longrightarrow A_XB_Y\,(s)$$

Nucleation is the least understood process in precipitation. Three main types of nucleation occurs in chemical precipitation: Primary homogeneous or heterogeneous or secondary. Homogeneous nucleation occurs in the absence of solid interface while heterogeneous nucleation occurs in the presence of foreign seed surfaces and secondary nucleation in the presence of a solute particle interface. The dominance of each type of nucleation varies with the precipitation conditions.

In homogeneous nucleation of small clusters a large fraction of atoms is present at the surface of the particles thus having higher potential energy than in the interior of the particles due to fewer and weaker bonds. The free energy of these small aggregates is the result of free energy due to the new surface and the formation of new solid. Most nucleation in precipitation methods is in practice likely to be heterogeneous since contact with vessel, stirrer is difficult to avoid. Nucleation on a foreign surface has a lower surface energy leading to a lower critical supersaturation. Secondary nucleation results from the presence of crystals in solution and can be divided into three classes: apparent, true and contact. Apparent refers to small fragments washed from the surface of seeds. True secondary nucleation occurs due to the presence of particles in solution. Contact secondary nucleation occurs when a growing particle contacts walls, stirrer, etc. producing new particles. Contact nucleation is often the most important nucleation mechanism and depends on rotation speed, particle mass density and saturation ratio.

4.2.2.2 Particle Growth

After a particle is nucleated, it can grow by several different mechanisms. The kinetics of the growth mechanism determines the structure and particle size distribution. On a macroscopic level, mass transport usually limits the particle growth while heat transfer is so fast that it controls the growth only at a very high heat of

crystallization. Diffusion controlled growth is described by diffusion of solvated ions to the surface and diffusion of solvent and other coordination ions away from the surface. The supersaturation driving force can be written as S-S(r*) if the particles are small. If S-S(r*) is positive a particle will precipitate from solution and when S-S(r*) is negative particles smaller than size r will dissolve and particles larger than r* will grow. This dissolution of fine particles and re-precipitation of larger particles is called Ostwald ripening. Ripening occurs in batch reactors because the supersaturation ratio, S, decreases with time. At high supersaturation, nucleation produces large numbers of fine particles.

Impurities can change the crystal habit drastically, especially ionic surfactants which by adsorbing on the surface of a crystal can change the kinetics. Impurities can reduce the supply of material to the surface, reduce the specific surface energy or block surface sites. Ionic surfactants adsorb on to the surfaces with opposite charges and can limit the growth of particles in some directions.

4.2.2.3 Agglomeration

In chemical methods, the agglomeration time is long compared to the confined growth zone in vaporization methods. Normally, crystals do not occur as single discrete units but they form bigger clusters. There are two main classes of agglomeration; primary agglomeration results from the faulty growth of crystals and secondary growth are due to crystal-crystal interactions. There are two cases of secondary aggregation. Particles can aggregate by Brownian motion or shear induced aggregation. In the first case, the diffusion of particles by Brownian motion causes collisions and in the latter case fluid movement causes particle collisions.

4.2.2.4 Drying

The precipitation methods involve separation of solid phase from the liquid reaction media. Drying requires simultaneous heat and mass transfer. These processes are dependent on the temperature and partial pressure of the solvent in the atmosphere. Depending on the kinetics of the drying of the boundary layer surrounding the green body and the pores different stresses are induced in the material. The wet green body has a compressive capillary force which holds it together. During drying, this capillary induced tension is present if flows keep the surface wet. This flow arises from the rearrangement of particles in the green body. This capillary force disappears as the liquid is evaporated. During drying the green body is susceptible to non-uniform stresses due to the pressure gradient of the flow of liquid during shrinkage and the escaping gases or the differential thermal expansion of the ceramic due to temperature gradients in the green body.

The co-precipitation method is relatively easy to scale-up. Compared to other chemical method, co-precipitation is a very friendly synthetic method. Not only are there fewer toxic byproducts but the temperatures required during the initial synthesis are not as extreme. The main advantage of precipitation is, in comparison to solid state reaction methods is that it rejects most of the impurities to the solution during the formation of solid product. Figure 4.3 represents the Flow chart of the co-precipitation process.

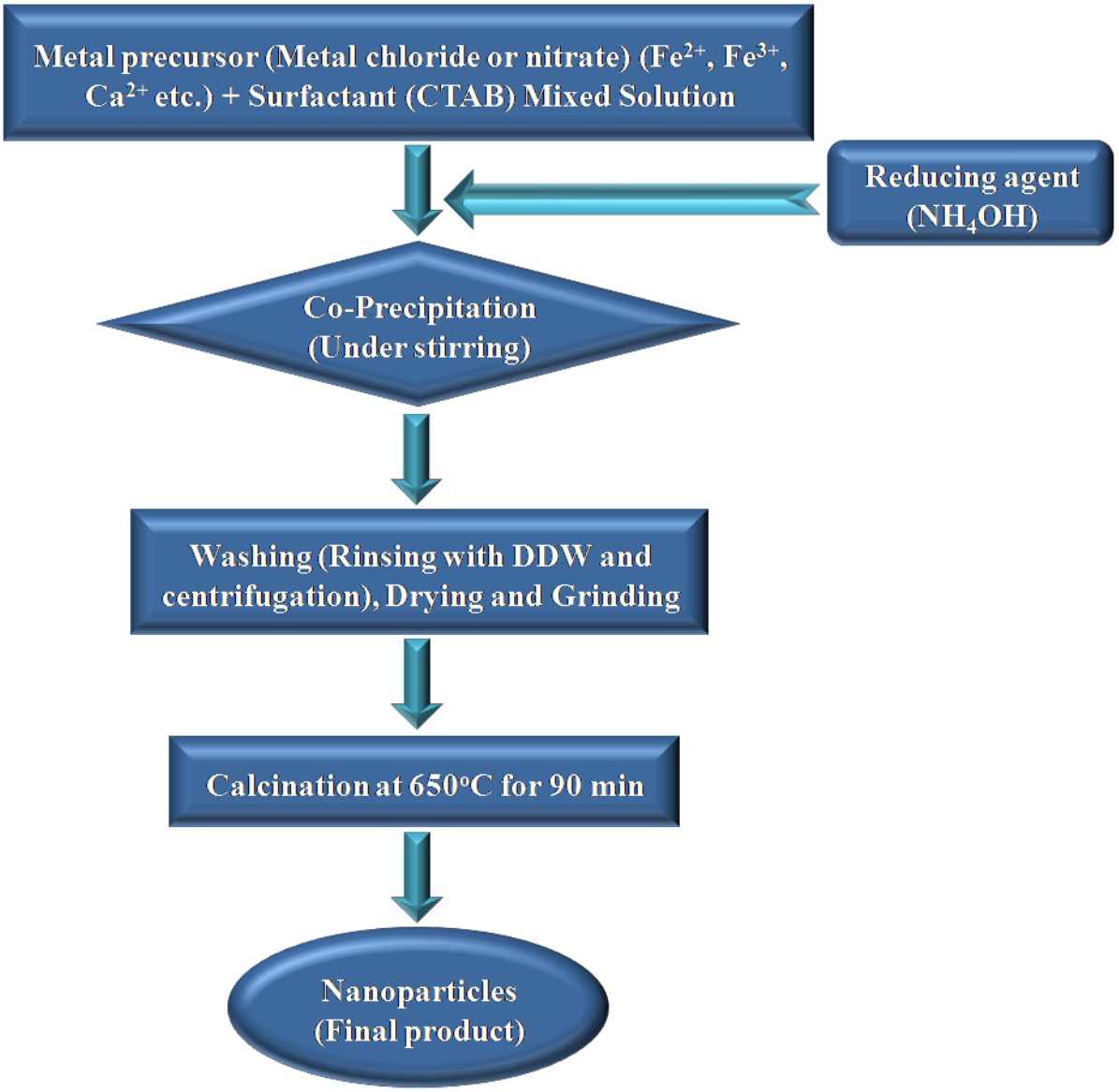

Figure 4.3 Flow chart of the co-precipitation process

In this present work, we have synthesised Fe_2O_3-Gd_2O_3, $NiFe_2O_4$-Gd_2O_3, Gd_2O_3-NiO and Gd_2O_3-$NiFe_2O_4$ core-shell nanosystems were synthesised by polyol method and HAP, Fe_2O_3 were synthesised from co-precipitation method for the analysis of dielectric and magnetic studies.

4.3 Characterisation of Synthesised Materials

Scientific studies have been carried out through experiments and various measurement techniques. In order to understand the physical and chemical behaviour of the materials, different aspects of the materials like the structural, microstructural, thermal, electrical, mechanical, optical properties etc. should be carried out. The basic experimental techniques along with their scope used in the present investigation are described in the following sections.

4.3.1 Thermo gravimetric analysis (TGA)

The mostly used thermal analysis includes thermo gravimetric analysis (TGA), differential thermal analysis (DTA) and differential scanning calorimetry (DSC). DTA and DSC are used to monitor the heat flow to and from a sample and to or from a reference as a function of temperature or time while the sample is subjected to a controllable temperature program, respectively. The TGA is a unique technique which is monitored as a function of temperature or time by means of the mass of the sample.

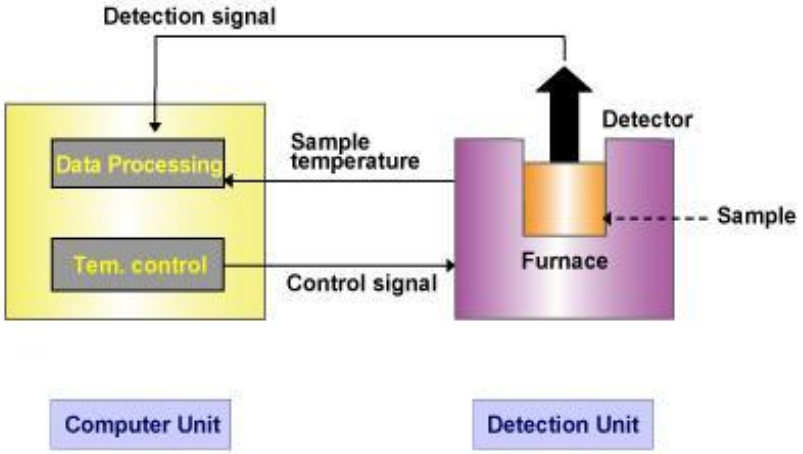

Figure 4.4 Schematic diagram of TGA/DTA

TGA was used in this study to determine decomposition, thermal stability and sintering behaviour of the prepared samples. In this measurement, a few milligrams of the sample were heated and the mass loss was monitored as a function of temperature. The measurements were performed in the temperature range 35 °C -1000 °C at a rate of 10 °C min^{-1} in air. TGA measurements were carried out using a SII Nanotechnology Inc., Japan, EXSTAR6200 thermal analyser. Figure 4.4 shows the schematic representation of the TGA technique which was used in this study.

4.3.2 X-ray Diffraction Method (XRD)

In 1912, German physicist Max Von Laue suggested with great insight that if the wavelength of X-rays is order of the interatomic distance (about 1 Å); the crystals could be a diffraction lattice for them whose wavelength is comparable with the lattice parameter. In that way, X-rays give information about the structure of crystalline materials. The interference within individual atoms affects the amplitude of the outgoing wave and scattering has a constructive interference in specific directions. However, the intensity integrated in all directions remains constant due to energy conservation. Figure 4.5 illustrates the reflection of X-rays by the atomic planes. Constructive interference or reflection is obtained when the path of the wave scattered of the lower of the two planes is longer by an integer number of wavelengths λ than that of the wave scattered of the upper plane. It is established in the Bragg‟s equation,

$$n\lambda = 2d_{(hkl)}\sin\theta \quad \ldots\ldots\ldots\ldots\ldots\ldots\ldots\ldots (4.1)$$

and gives the permitted angles of reflection θ, in terms of the wavelength λ of the radiation used and the spacing of the reflecting planes d, n is an integer, analogous to the order of diffraction from a grating, so that "nλ" is the path difference between

waves scattered from adjacent lattice planes with equivalent indices. Each crystalline solid has its unique characteristic XRD pattern which may be used as a "fingerprint" for its identification. Once the material has been identified, X-ray crystallography may be used to identify the crystal structure and the unit cell parameters.

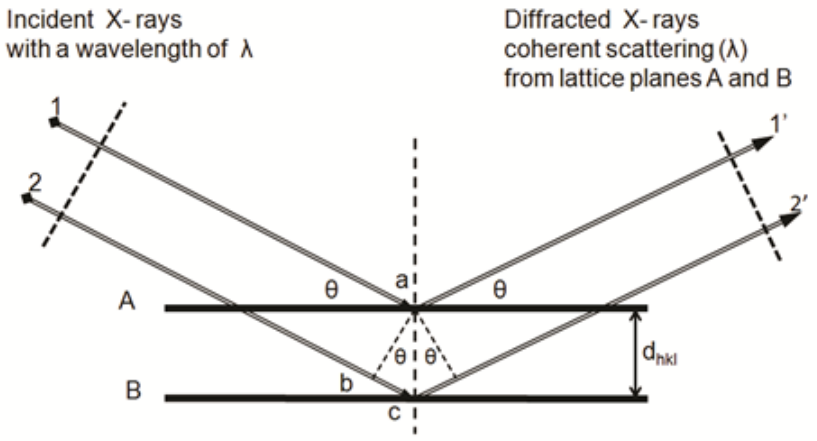

Figure 4.5 Geometric diagram of the reflection of X-rays by two planes

In our work, we obtain other specific results from XRD: Identification of crystal phase of the corresponding material, recognition of amorphous materials in nanocrystalline mixtures. The X-ray diffraction (XRD) measurement of the samples is taken at room temperature by X-ray diffractometer (Rigaku Miniflex-II; USA) in the range of Bragg angles $10^o \leq 2\theta \leq 70^o$ with a scanning rate of 0.02^o per step using Cu target with Ni filter and radiation of CuK_α (λ=1.5405 A^o). Identification of the phases was carried by comparison with the compiled diffraction patterns by the Joint Committee for Powder Diffraction Standards (JCPDS) [22].

4.3.3 Scanning Electron Microscopy (SEM)

In modern material science research, scanning electron microscope (SEM) is widely used powerful tool. SEM produces an image with marked three-dimensional appearance. It produces micrographs by scanning the surface of a specimen with a small electron probe (a beam of electron) synchronous with an electron beam from a

source. The contrast is due to the topographical variations and atomic number differences in the specimen. The SEM is capable of examining a relatively large field of view, thus giving sufficient information of the structure and its uniformity, topographical details of a surface with clarity and detail, the particle aspect ratio and the regularity of pattern arrays [23-25]. The basic units of SEM are: (a) electron-optical columns together with appropriate electronics, (b) the vacuum system, which includes the specimen chamber and stage, (c) signal detection and display systems. The electron column contains magnetic lenses whose function is to demagnify the electron beam. Two sets of scanning coils are incorporated in the SEM. The scanning coils are coupled with appropriate scan generator to cause the beam to be deflected over the specimen surface in a roster like pattern. The specimen chamber is designed such that specimen orientation is rapid and provides many movements. The normally attained orientations in the specimen stages are translation, 360^{o} rotation and provision for tilting the specimen.

The detection system used in SEM depends on the interaction of primary electron beam with the specimen. The different effects are secondary electron emission, reflected or back-scattered electron current, x-ray production and cathodoluminescence. All of the signals can be detected, amplified and used to control the brightness of a cathode ray tube (CRT). The deflection of the electron beam in the CRT is controlled by the same scan generator which determines the position of the electron beam on the sample. For microscopic study the scanning electron micrograph of the samples under investigation are taken by a FEI Quanta 200 scanning electron microscope. All the samples are sputtered by gold using ion sputtering unit to increase the conductivity of the samples.

4.3.4 Energy Dispersive X-ray (EDX) Analysis

EDX analysis stands for energy dispersive x-ray analysis. It is sometimes referred to also as EDS or EDAX analysis. It is a technique used for identifying the elemental composition of the specimen, on an area of interest thereof. The EDX analysis system works as an integrated feature of a scanning electron microscope (SEM).

During EDX Analysis, the specimen is bombarded with an electron beam inside the scanning electron microscope. The bombarding electrons collide with the specimen atom‟s own electrons, knocking some of them off in the process. A position vacated by an ejected inner shell electron is eventually occupied by a higher-energy electron from an outer shell. To be able to do so, however, the transferring outer electron must give up some of its energy by emitting an X-ray. The amount of energy released by the transferring electron depends on which shell it is transferring from, as well as which shell it is transferring to. Furthermore, the atom of every element releases X-rays with unique amounts of energy during the transferring process. Thus, by measuring the energy of the X-rays emitted by a specimen during electron beam bombardment, the identity of the atom from which the X-ray was emitted can be established.

The output of an EDX analysis is an EDX spectrum, which is a plot of how frequently an X-ray is received for each energy level. An EDX spectrum normally displays peaks corresponding to the energy levels for which the most X-rays had been received. Each of these peaks is unique to an atom and therefore corresponds to a single element. The higher a peak in a spectrum, the more concentrated the element is in the specimen. An EDX spectrum plot not only identifies the element corresponding to each of its peaks, but the type of X-ray to which it corresponds as well. For

example, a peak corresponding to the amount of energy possessed by X-rays emitted by an electron in the L-shell going down to the K-shell is identified as a Kα peak. The peak corresponding to X-rays emitted by M-shell electrons going to the K-shell is identified as a Kβ peak as shown in Figure 4.6.

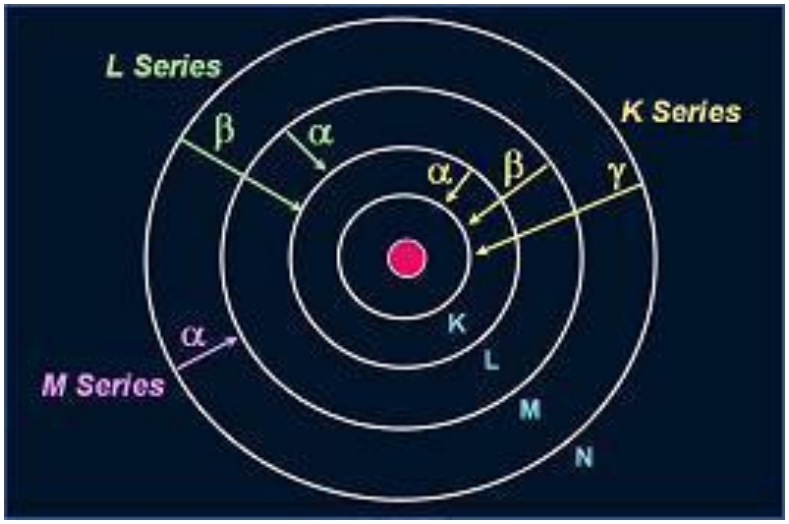

Figure 4.6 Emission of X- rays

4.3.5 Transmission Electron Microscopy (TEM)

The transmission electron microscope works similarly as an optical analogue to the conventional light microscope. Electron wavelength allows higher magnification and better resolutions. The electrons are accelerated under a potential of up to 100 keV or higher. The electron beam is focused by several electromagnetic lenses on a single, spot or element at a very thin sample and detecting those transmitted through it hitting the phosphor screen on the other side. After interaction of electrons with the sample one is able to obtain a map of the local densities with lighter and darker areas, as well as diffraction information of crystals. Sample preparation is crucial, and usually involves placing very dilute particle suspensions onto carbon-coated copper grids. Another useful technique is imbedding the particle

in a solid organic polymer, slicing very thin sections, and passing the electron beam through the section.

Transmission electron microscopy (TEM) was performed in this work with a TECHNAI G^2 TF20ST. We added small amount of nanoparticle and 5 ml organic solvent (ethanol, acetone etc.) in a glass vial and sonicated for 40 minutes. One drop of the resulting suspension was dropped on carbon coated copper grid. The micrographs showing dispersed particles with high contrast (dark) respect to the carbon film (bright background).

4.3.6 UV-Visible Absorption Spectroscopy

The absorption of ultraviolet (UV) or visible radiation generally results from excitation of bonding electrons. The wavelengths of absorption bands can be correlated with the type of bonds in the materials under study. There are a number of different electronic excitations that can take place in these compounds. These can be either localized intra-atomic excitations or band to band transitions. The band gap transitions are easily identified by the large intensity of their absorptions and the broadness of the peak. The band gap energies can be estimated by extrapolating the linear portion of the band absorption peak to zero absorbance.

The UV-Visible absorption spectrum of the sample at room temperature was measured by a Shimadzu UV-Visible spectrometer (UV-2401; Japan) over a wavelength range from 300 to 600 nm.

4.3.7 Raman Spectroscopy

Chemical bonds between atoms in a molecule or a crystal are not rigid. Raman spectroscopy is a spectroscopic technique used to study vibrational, rotational and low frequency modes in a material. Raman Effect is caused by modulation of susceptibility of the medium by vibrations. Vibrations are characteristic for a material and inelastic scattering $\omega = (k/\mu^*)^{1/2}$, where k is force constant and μ^* is reduced mass. It involves the coupling between incident photons and quasiparticle excitons such as phonons, magnons and electronic single particle within a sample. In crystalline solids, Raman effect deals with phonons. A phonon is Raman active if the first derivative of the polarizability with respect to the vibrational normal co-ordinate has a non-zero value. The possible Raman modes depend on the symmetry of the solid considered. Raman scattering by an anisotropic crystal gives information on the crystal orientation. Number of lattice vibration modes of a crystal with „n‟ number atoms per unit cell is 3n; in which 3 are acoustic modes and remaining 3n-3 are optic modes. These optic modes are categorized into infrared active, Raman active and silent (neither Raman nor IR active) modes. For a mode to be IR active, dipole moment should change with the vibration. According to the exclusion principle, no mode is both Raman and IR active for centro-symmetric structures. Micro-Raman scattering spectrum of the sample was measured at room temperature at an excitation wavelength of 488 nm using a Lab-RAM HR 800 (Jobin Yvon; France) Raman spectrometer.

4.3.8 Dielectric Study

Alternating current impedance spectroscopy (ACIS) is used to study the dielectric properties of the materials. ACIS allows measuring the capacitance (C) and loss tangent (tanδ) in a wide frequency range at various temperatures. From the measured capacitance and loss tangent, we can calculate the four basic dielectric functions. The real and imaginary parts of dielectric constant are obtained from the relation $\varepsilon' = C/C_0$ and $\varepsilon'' = \varepsilon' \tan\delta$ respectively. From these two parameters other dielectric functions are calculated.

For the dielectric measurement, the sintered pellets are placed between the gold electrodes. After that, the pellet is connected to an impedance meter (Hioki3532 LCR Hightester) (Figure 4.7) for the measurement of capacitance and loss tangent in the frequency range from 100 Hz to 1 MHz as a function of temperature. The Eurotherm 2216 temperature controller is used to control the temperature of the sample. All the dielectric data are taken while heating at a rate of 0.5 ^{o}C min^{-1}.

Figure 4.7 Hioki 3532 Impedance Meter

4.3.9 Vibrating Sample Magnetometer (VSM)

Magnetic characterisation of the NPs was carried out using vibrating sample magnetometer (VSM). To describe VSM in the most basic sense, a sample is placed in a uniform constant magnetic field. If the sample is magnetic, this constant magnetic field will magnetize the sample by aligning the magnetic domains or magnetic spins with the field. If the sample vibrates in a sinusoidal motion, an electrical signal can be induced between two coils (pick-up coils). This signal has the same frequency of vibration and the amplitude is proportional to the magnetic moment of the material. A vibrating sample magnetometer (ADE make EV9 Model) was used for magnetic measurements up to 20 kOe at room temperature.

4.3.10 Electron Spin Resonance Spectroscopy (ESR)

Electron spin resonance (ESR) or electron paramagnetic resonance (EPR) spectroscopy is a technique used for studying chemical species that have one or more unpaired electrons. The basic physical concepts of ESR are analogous of nuclear magnetic resonance (NMR), but it is electron spins that are excited instead of spins of atomic nuclei. The electron spin, S = 1/2, can be degenerate into two different quantum levels (m_s S= 1/2) when a magnetic field, H_0 is apply to the electron (i.e, of the material to be studied). Then, the difference energy, ΔE, needed to excite an electron from the down (m_S = - 1/2) level to the upper (m_S = + 1/2) level is defined as the difference of the energy of these two quantum states (equation 4.2). Figure 4.4 shows the schematic representation the resonance of free electron by the external field.

$$\Delta E = g_e \mu_B H_0 \text{ …….. (4.2)}$$

where g_e is the electron g-factor or gyromagnetic constant equals to 2.0023193 for a free electron and μ_B is the Bohr magneton and is equal to $9.2740 * 10^{-24}$ J T^{-1}; and H_0

indicates the external magnetic field.

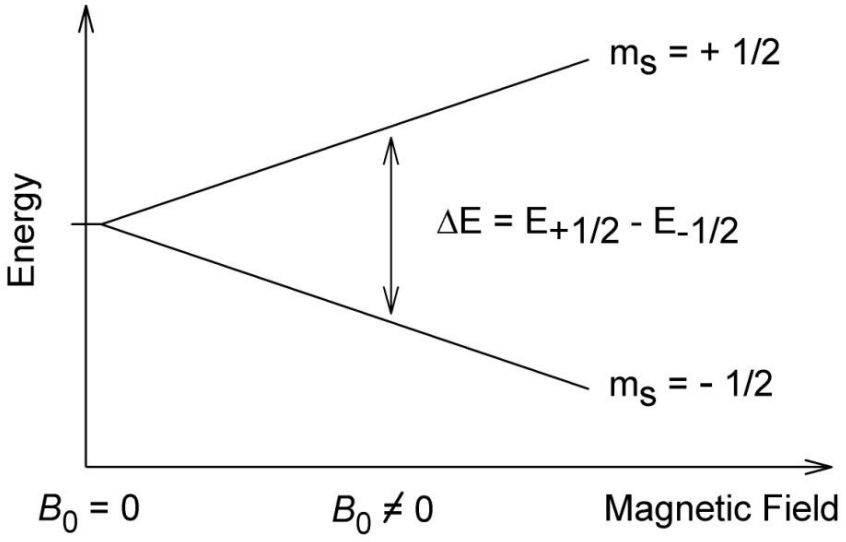

Figure 4.8 Resonance of a free electron

With analogous interpretation, the energy gap can be defined as the related absorbed/emitted electron magnetic radiation energy for resonance condition, $\Delta E = h\nu$ where are h the Plank's constant and ν the electromagnetic frequency. Then,

$$h\nu = ge\ \beta_B\ H_0 \quad \ldots\ldots\ldots \quad (4.3)$$

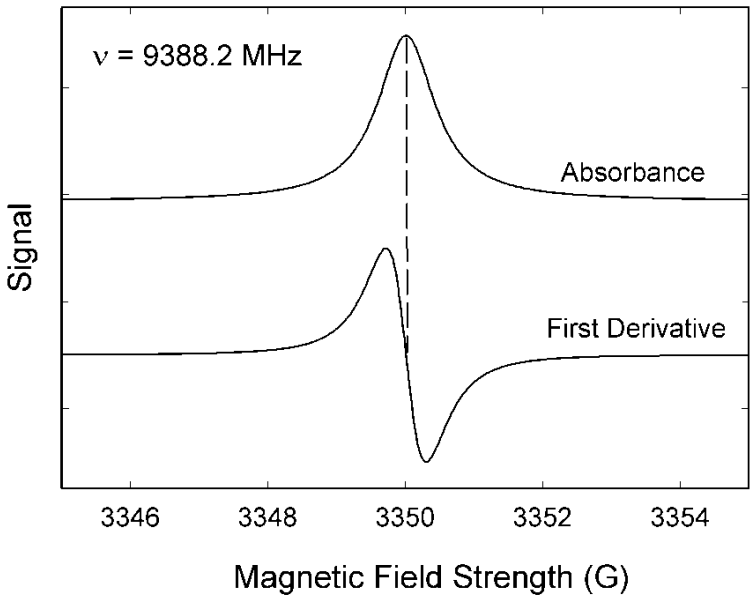

Figure 4.9 ESR spectrum for absorbance and its first derivative

The most common way to depict ESR spectra is the first derivative of the absorbance spectra (Figure 4.9). The parameters that characterise the resonance signal are the resonance field Hr, the line width, ΔH, and the spectrum intensity. The spectrum intensity value is proportional to the amount the specific ion in the sample resonating at a given frequency field. Hr is defined as the resonance field for specific specimen absorption. In short, this value should vary only with the magnetic field applied. But for exchange-coupled systems (i.e., exchange bias or spring-magnets systems) the extra anisotropy created due to the interphase coupling generates an additional field that can increase or reduce the Hr value. Also, solving the equation 4.3 using the specific Hr value the gyromagnetic factor can be obtained. The gyromagnetic factor for a non-isolated electron (i.e., electron confined in atom or molecule) differs from the well known value of 2.0023193. Then, the magnitude of the change with respect to the standard value of g gives information about the nature of the atomic or molecular orbital containing the unpaired electron.

The shape or profile of the resonance lines are determined by the type of interactions between the spin system and its environment, while the line width, ΔH, depends on the intensity of interaction and the relaxation time. ΔH is measured as the distance between the two main peaks present into the first derivative absorbance. The line width is related to the width of upper energy level (m_s = + 1/2) and is strongly related with the energy indeterminacy of the upper level, or half live time of the electrons in this quantum state.

EPR is a powerful tool in investigation of magnetic properties and spin dynamics in solids. The position of the EPR line depends on the ratio of magnetic induction to ν and the effective gyromagnetic ratio (g). From the width and shape of the resonant line we can obtain detailed information on magnetic and electronic state

of the element. The gyromagnetic factor is strongly related to the crystallographic structure of the atom under study, thus rendering information on the phase containing the resonant atom. On the other hand, we have investigated the resonant field (Hr), line width (ΔH), and the spectrum intensity, as a function of the temperature. Their dependence with the temperature allows to study the spin dynamics the material in solid state and to extract the ΔH factor which is strongly related to magnetic environment of the material, thus with information on the anisotropy and the exchange energy. In the present work, variable temperature EPR spectra were recorded from 300 K to 110 K during cooling by a Bruker EMX plus spectrometer operating at X-band (frequency = 9.43 GHz) with 100 kHz magnetic field modulation. Form which the resonance field, line width and spectrum intensity have been obtained.

4.3.11 Mossbauer Spectroscopy

Mossbauer spectroscopy is a spectroscopic technique based on the Mossbauer effect. This effect consists in the recoil-free, resonant absorption and emission of gamma rays in solids. Like NMR spectroscopy, Mossbauer spectroscopy probes tiny changes in the energy levels of an atomic nucleus in response to its environment. Typically, three types of nuclear interaction may be observed: an isomer shift, also known as a chemical shift; quadrupole splitting; and, magnetic or hyperfine splitting, also known as the Zeeman Effect. Due to the high energy and the extremely narrow line widths of gamma rays, Mossbauer spectroscopy is one of the most sensitive techniques in terms of energy (and hence frequency) resolution, capable of detecting change in just a few parts per 10^{11}. It is formed by three main parts; a source that moves back and forth to generate a doppler effect, a collimator that filters out non-parallel gamma rays and a detector (Figure 4.10).

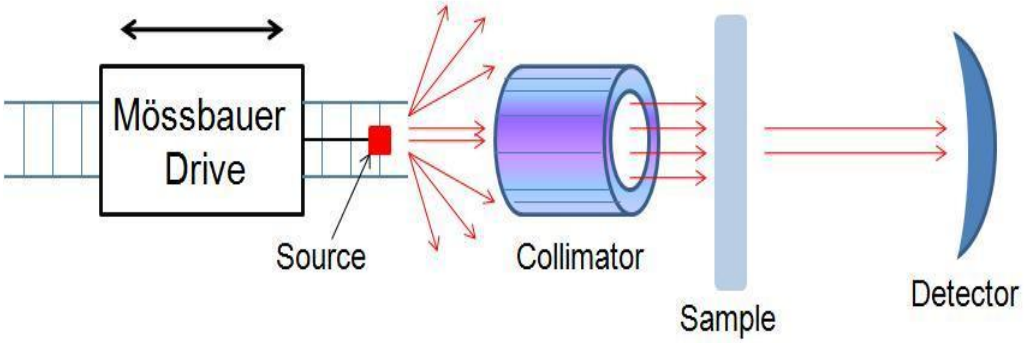

Figure 4.10 Schematic view of Mossbauer spectrometer

During Mossbauer absorption spectroscopy, the source is accelerated through a range of velocities using a linear motor to produce a Doppler effect and scan the gamma ray energy through a given range. A typical range of velocities for 57Fe, for example, may be ±11 mm/s. In the resulting spectra, gamma ray intensity is plotted as a function of the source velocity. At velocities corresponding to the resonant energy levels of the sample, a fraction of the gamma rays are absorbed, resulting in a drop in measured intensity and a corresponding dip in the spectrum. The number, positions and intensities of the dips (also called peaks; dips in transmitted intensity are peaks in absorbance) provide information about the chemical environment of the absorbing nuclei and can be used to characterise the sample. 57Fe Mossbauer spectra were recorded using a FAST Comtec (Germany) spectrometer at room temperature in transmission geometry with a 25 mCi 57Co gamma ray source in rhodium matrix in this work.

References

1. C. Feldmann and C. Metzmacher, J. Mater. Chem. 11 (2001) 2603.
2. P. Toneguzzo, G. Viau, O. Acher, F. Guillet, E. Bruneton, F. F. Vincent and F. Fievet, J. Mater. Sci. 35 (2000) 3767.
3. S. Sun, C. B. Murray, D. Weller, L. Folks and A. Moser, Science, 287 (2000) 1989.
4. P. Toneguzzo, G. Viau, O. Acher, F. F. Vincent and F. Fievet, Adv. Mater. 10 (1998) 1032.
5. F. Fievet, F. F. Vincent, J. P. Lagier, B. Dumont and M. Figlarz, J. Mater. Chem. 3 (1993) 627.
6. J. R. Joseyphus, D. Kodama, T. Matsumoto, Y. Sato, B. Jeyadevan and K. Tohji, J. Magn. Magn. Mater. 310 (2007) 2393.
7. T. Sugimoto and E. Matijevic, J. Colloid Interface Sci. 74 (1980) 227.
8. A. Chastellain, A. Petri and H. Hofmann, J. Colloid Interface Sci. 278 (2004) 353.
9. J. P. Jolivet, Metal Oxide Chemistry and Synthesis: From Solutions to Solid State (New York: Wiley) (2000).
10. P. Tartaj, M. D. Morales, S. V. Verdaguer, T. G. Carreno and C. J. Serna, J. Phys. D: Appl. Phys. 36 (2003) R182.
11. P. Tartaj, M.P. Morales, T. G. Carreno, S. V. las-Verdaguer and C. J. Serna, J. Magn. Magn. Mater. 290 (2005) 28.
12. D. K. Kim, Y. Zhang, W. Voit, K.V. Rao and M. Muhammed, J. Magn. Magn. Mater. 225 (2001) 30.
13. D. K. Kim, M. Mikhaylova, Y. Zhang and M. Muhammed, Chem. Mater. 15 (2003) 1617.
14. C. L. Lin, C. F. Lee and W. Y. Chiu, J. Colloid Interface Sci. 291 (2005) 411.
15. Z. P. Xu, Q. H. Zeng, G. Q. Lu and A. B. Yu, Chem. Eng. Sci. 61 (2006) 1027.
16. H. Lee, E. Lee, D. K. Kim, N. K. Jang, Y. Y. Jeong and S. Jon, J. Am. Chem. Soc. 128 (2006) 7383.
17. S. Mohapatra, N. Pramanik, S. Mukherjee, S.K. Ghosh and P. Pramanik, J. Mater. Sci. 42 (2007) 7566.
18. D. K. Kim, M. Mikhaylova, F. H. Wang, J. Kehr, B. Bjelke, Y. Zhang, T. Tsakalakos and M. Muhammed, Chem. Mater. 15 (2003) 4343.

19. C. Bergemann, D. M. Schulte, J. Oster, L. Brassard and A. S. Lubbe, J. Magn. Magn. Mater. 194 (1999) 45.
20. R. M. Cornell, U. Schwertmann, The Iron Oxides: Structure, Properties, Reactions, Occurrences and Uses, second ed. Wiley-VCH, Weinheim, (2003).
21. S. Laurent, D. Forge, M. Port, A. Roch, C. Robic, L. V. Elst and R. N. Muller. Chem. Rev. 108 (2008) 2064.
22. JCPDS-ICDD, Joint committee for powder diffraction standards, International Center of Diffraction Data (1997).
23. J. R. Jurado, M. T. Colomer and J. R. Frade, J. Am. Ceram. Soc. 83 (2000) 2715.
24. F. D. Morrison, D. C. Sinclair and A. R. West, J. Appl. Phys. 86 (1999) 6355.
25. S. Ananta and N. W. Thomas, J. Eur. Ceram. Soc. 19 (1999) 2917.